Nanosheets

DOI: 10.1002/anie.201302891

Ultrathin Nanosheets of Half-Metallic Monoclinic Vanadium Dioxide with a Thermally Induced Phase Transition**

Tao Yao, Liang Liu, Chong Xiao, Xiaodong Zhang, Qinghua Liu, Shiqiang Wei, and Yi Xie**

Monoclinic vanadium dioxide, VO_2(M), is an archetypal correlated material that exhibits a first-order phase transition, from a low-temperature insulating monoclinic (M) to high-temperature metallic rutile (R) phase, which is accompanied by a switch in the optical transmission/blocking in the infrared (IR) region.[1–3] These dramatic thermally induced switches in electrical resistivity and optical response endows VO_2 with exciting prospective applications as a field-effect transistor and as smart window materials.[4,5] As a transition-metal oxide, however, use in spintronics, which exploits both the intrinsic spin and charge of electrons, should also be highly desired.[6] An ideal component for spintronic devices is half-metallic material, which is metallic for one spin channel and insulating for the other, resulting in 100% spin polarization.[7] Among oxides, only the bulk CrO_2 and Fe_3O_4 have been found to exhibit half-metallicity.[8] To the best of our knowledge, the half-metallic character in the pristine VO_2(M) is scarcely reported.

Recently, ultrathin two-dimensional (2D) nanosheets that have an exceptionally small thickness and one-dimensional quantum confinement have received a surge of interests owing to their fascinating physical and chemical properties.[9,10] It has been predicted theoretically that reducing the dimension of some bulk materials to 2D atomically thin nanosheets will bring about half-metallicity.[11–14] For example, Son et al. has predicted half-metallicity in nanometer-scale graphene ribbons by using first-principles calculations.[11] Pardo et al. predicted that half-metallic state with a semi-Dirac point appears in few-layer VO_2(M) confined within insulating TiO_2.[12] However, the half-metallicity in low-dimensional oxide systems has only been theoretically predicted to date. On the other hand, methods for preparing a freestanding ultrathin VO_2(M) nanosheet with the thicknesses of less than 5 nm have not been available.[15] Particularly, even the pure bulk VO_2(M) phase is notoriously difficult to synthesize because of the existence of abundant oxide forms and polymorphism.[16,17] The most widely used solid-state synthesis usually requires the rigid synergic effects of high-temperature post-treatment and narrow range of oxygen partial pressures. Moreover, a conventional, simple intercalation–deintercalation method to obtain nanosheets is mainly limited to layered compounds, which is obviously unsuitable to achieve the exfoliation of bulk VO_2(M) with a non-layered structure and little anisotropy. For another monoclinic polymorph VO_2(B), a quasi-layered compound having the strongly covalent bonding between the layers, we have recently developed a novel intercalation–exfoliation/deintercalation strategy by insertion of lithium ions and molecules (H_2O) to obtain nanosheets.[18] To seek possible ways for overcoming these difficulties in preparing ultrathin VO_2(M) nanosheets, the temperature-dependent structural phase transition (SPT) characteristic of VO_2(M) gives us some hints, as the lattice will be swelled in some specific directions during the reversible SPT across a critical temperature (T_C, around 68 °C). When transiting from the M to R phase (Supporting Information, Figure S2), the VO_2 structure shows an increased symmetry, and the lattice constants of the R phase are elongated with respect to the M phase by about 0.6% and 0.4% along the a_R and b_R axis, respectively.[19] This reminds us that SPT-induced lattice expansion and anisotropic strain could weaken the binding strength and thereby assist the deintercalation.

Herein, considering the special thermally induced SPT character possessed by VO_2(M), we propose a SPT-assisted synthetic strategy to achieve single-crystalline ultrathin VO_2(M) nanosheets with a thickness of about 3 nm. Bulk VO_2(M) is synthesized as the precursor, and the synthetic route is summarized in Figure 1a, which basically involves two steps: chemical lithiation of VO_2(M) in LiCl solution and exfoliation–deintercalation of VO_2(R) in DMF/H_2O solution. Details of the synthesis and characterization are provided in the Supporting Information. It was found that below or above the T_C, both of these two process would produce different phases and shapes for the intermediates and the final products. When the lithiation process is carried out at the temperatures lower than T_C, the intermediate shows a lamellar morphology and remains in the pure monoclinic phase. If the lithiation is performed above T_C, the impurity phases of V_6O_{13} are formed. Therefore, the intermediates lithiated in M phase

[*] Dr. L. Liu,[+] C. Xiao, X. D. Zhang, Prof. Y. Xie
Hefei National Laboratory for Physical Science at Microscale, University of Science and Technology of China
Hefei, Anhui, 230026 (P. R. China)
E-mail: yxie@ustc.edu.cn
Dr. T. Yao,[+] Dr. Q. H. Liu, Prof. S. Q. Wei
National Synchrotron Radiation Laboratory
University of Science and Technology of China
Hefei, Anhui, 230029 (P. R. China)
E-mail: sqwei@ustc.edu.cn
Dr. L. Liu[+]
Automotive Engineering Research Institute, JiangSu University
Zhenjiang, Jiangsu, 212013 (P. R. China)
[+] These authors contributed equally to this work.

[**] The research was financially supported by the National Basic Research Program of China (2009CB939901), the Chinese Academy of Science (XDB01020300), and the National Natural Science Foundation of China (11079004, 90922016, 11135008, and U1232132).
Supporting information for this article is available on the WWW under http://dx.doi.org/10.1002/anie.201302891.

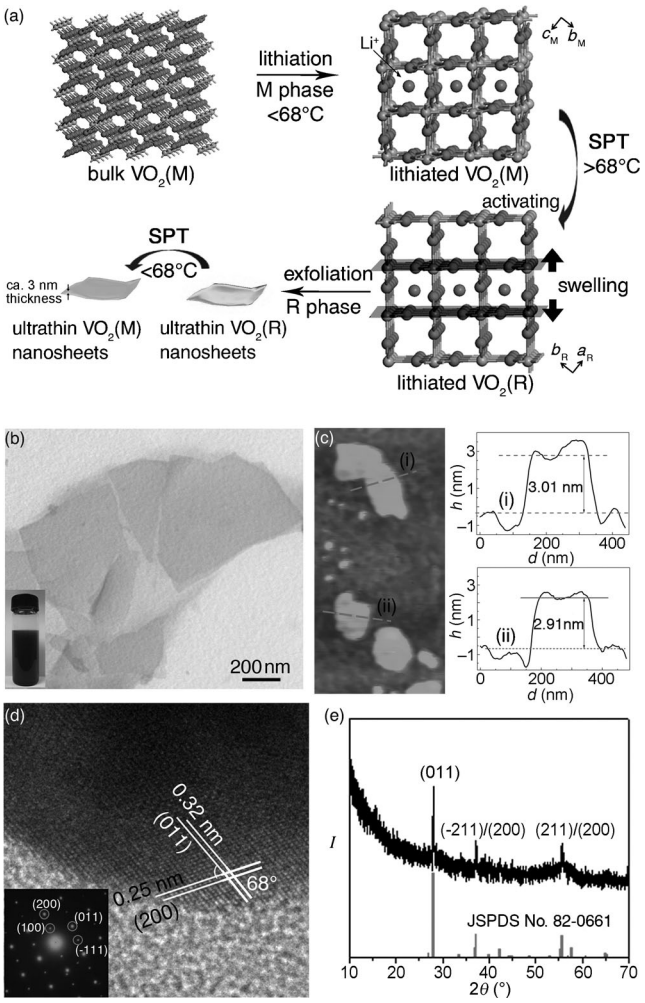

Figure 1. a) The SPT-assisted intercalation–deintercalation strategy for synthesizing freestanding ultrathin VO_2(M) nanosheets. b) TEM image of ultrathin VO_2(M) nanosheets. Inset: the colloidal dispersion. c) AFM image corresponding height profiles for nanosheets. d) HRTEM image of an nanosheet and the corresponding SAED pattern. e) XRD pattern of VO_2(M) nanosheets and the reference pattern of JCPDS card no. 82-0661 for bulk VO_2(M).

are used for the following ultrasonic exfoliation/deintercalation process. However, directly exfoliating the lithiated VO_2(M) intermediates at room temperature (below T_C) would produce the thick VO_2(M) nanoplates with a thickness of about 17.16 nm (Supporting Information, Figure S3). To obtain ultrathin nanosheets with the thickness of about 3 nm, we find that lithiated VO_2(M) should firstly experience a SPT process into the R phase. In this process, the lattice spacing is swelled as seen from the c_R direction, and thus subsequent exfoliation/deintercalation of lithiated VO_2(R) provides a convenient way to obtain ultrathin VO_2(R) nanosheet. As the SPT between VO_2(M) and VO_2(R) is fully reversible, ultrathin VO_2(M) nanosheets are achieved through cooling the ultrathin VO_2(R) nanosheets to room temperature. Taking the above together, M-phased lithiation followed by R-phased exfoliation/deintercalation is confirmed to be an effective strategy to produce ultrathin VO_2(M) nanosheets.

The ultrathin nanosheets thus obtained have been fully characterized by various techniques. Figure 1b shows a transmission electron microscopy (TEM) image of the obtained product, revealing the uniform freestanding and large-area sheet-like morphology with lateral size of 200–500 nm, whereas the inset magnified TEM image clearly revealed their high crystallinity. Separation of the supernatant infers the formation of stable and homogeneous VO_2(M) nanosheets (Figure 1b, inset). The thickness of the as-obtained ultrathin nanosheets was determined by tapping-mode atomic force microscopy (AFM) (Figure 1c). The corresponding height profiles of two typical piece of nanosheets show a smooth 2D sheet with the thickness of 2.91 and 3.01 nm, which is very close to the height of 2.61 nm along the [h11] direction for circa 6 single-layer VO_2(M) slabs. Statistical results (Supporting Information, Figure S4) of the size for the ultrathin nanosheets confirm the thickness of about 3 nm with a yield of more than 90%. The single-crystalline feature of the VO_2(M) nanosheets is verified by high-resolution TEM and the corresponding selected-area electron diffraction (SAED) pattern (Figure 1d). Two lattice fringes of 3.2 Å and 2.5 Å correspond to the (011) and (200) lattice planes of VO_2(M), respectively. The SAED pattern (Figure 1d, inset) can be indexed along the $[00\bar{1}]$ zone axis projection.[20,21] Owing to the fact that it is hard to perform the X-ray diffraction (XRD) characterization on a single ultrathin structure, a layer-by-layer assembly strategy was adopted to fabricate a nanosheet-based film on which the XRD was performed to elucidate the phase structure of the VO_2(M) nanosheet. It can be seen that all the diffraction peaks in the XRD pattern as shown in Figure 1e could be readily indexed to the pure monoclinic VO_2 (JCPDS No. 82-0661), exhibiting strong (h11), for example (011), $(\bar{2}11)$, and (211) diffraction peaks. This not only revealed the high orientation of the VO_2(M) nanosheet-based film, but also illustrated that the VO_2(M) nanosheet had a highly [011] preferred orientation,[22] in accordance with the HRTEM analysis. EDS analysis showed that the nanosheets are mainly composed of V and O without any impurity element, with a V/O molar ratio of 1:1.8 (Supporting Information, Figure S5), which is close to the stoichiometric ratio of VO_2. Therefore, we consider that within the detection limit of XRD, EDS, and XAFS (mentioned later), the existence of V–O byproducts in any other detectable form could be excluded, and the as-obtained ultrathin VO_2(M) nanosheet is of the pure monoclinic phase.

The underlying growth mechanism of the synthetic ultrathin nanosheet is in fact closely related to its characteristic thermally induced SPT. For the first lithiation process, it is reasonable that the direct lithiation in high-temperature solution would easily lead to the partial oxidization of the valent-sensitive VO_2. Thus, the lithiation of the bulk VO_2(M) under ambient conditions are favorable for the phase purity of the final product. To clarify the SPT-assisted exfoliation–deintercalation process, the XRD pattern for the bulk and the intermediates are shown in Figure 2 for comparison. After the insertion of Li ions, the crystal lattice spacing is slightly expanded, as can be reflected by the low-angle shift of the $(011)_M$ diffraction peak for the lithiated VO_2(M). The simulation gives the larger d_{011} of 3.209 Å for the lithiated

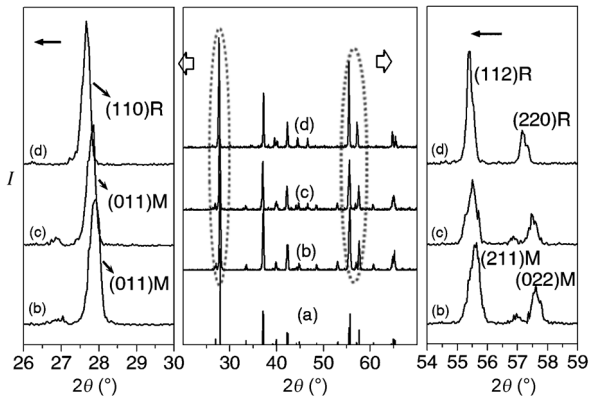

Figure 2. XRD patterns of a) standard VO_2(M), b) bulk VO_2(M), c) lithiated VO_2(M) intermediate, and d) lithiated VO_2(R) intermediate. The right and left panels magnify the shift of the diffraction peaks.

VO_2(M) compared with that (3.206 Å) for the bulk, while the Δd of 0.003 Å is too small for the next exfoliation–deintercalation. Across the SPT upon heating, these lithiated M-phased intermediates transform into the R phase, and the original $[011]_M$ direction becomes $[110]_R$.[23] The $(110)_R$ and $(112)_R$ diffraction peaks for the lithiated VO_2(R) further shifted toward the low-angle side. Consequently, the lattice spacing d_{110} for lithiated VO_2(R) is 3.233 Å, greatly larger than d_{011} for lithiated VO_2(M) by an amount of $\Delta d = 0.024$ Å. The enlargement of the lattice spacing decreases the interaction force between the layers, so that the energy required for the exfoliation–deintercalation of VO_2 in R phase is much lower as compared to the case of M-phased deintercalation.

To explore the atomic structures of the VO_2(M) nanosheets, we conducted X-ray absorption fine structure spectroscopy (XAFS) measurement at V K-edge. As shown in Figure 3a, the $k\chi(k)$ oscillation curve for the nanosheets shows a small reduction in amplitude and a little difference in spectral shape compared with that of bulk counterpart. Moreover, in the corresponding Fourier transforms (Figure 3b), two peaks at around 1.20 and 1.63 Å correspond to the chemical bonds of the V–O split, and the other two at around 2.12 and 2.86 Å are associated to the V–V1 and V–V2 bonds, respectively.[24] However, the peak intensities for the ultrathin nanosheets are weakened, and the V–V1 peak is broadened. Considering the thickness of 3 nm for the nanosheets, these structural differences are mainly from the surface structure distortion, while interior structure of nanosheets is almost the same as that of the bulk phase, resulting in the close features in the overall spectra between the bulk and nanosheets. The obtained surface structural parameters from the least-squares fits (Supporting Information, Table S1) all indicate the increased symmetry, which is characteristic of the SPT from monoclinic to rutile phases. For example, the bond lengths of dimerized V–V1 pairs in the V atomic chains evolve from 2.65 and 3.12 Å for the bulk to 2.73 and 2.99 Å for the nanosheets.

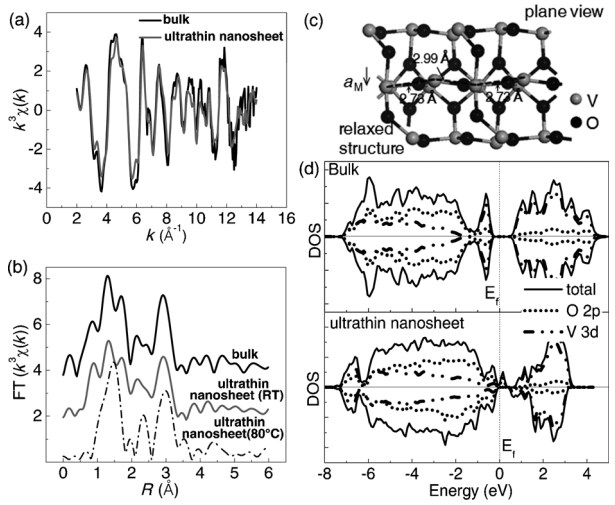

Figure 3. a) V K-edge extended XAFS oscillation function $k^3\chi(k)$ and b) the corresponding Fourier transforms for ultrathin VO_2(M) nanosheets. Data for bulk VO_2(M) are shown for comparison. c) The structural distortions of VO_2(M) nanosheets viewed along the a_M axis. d) The calculated band structures of bulk VO_2(M) and the six-monolayer VO_2(M) slab structure.

To unveil the changes of the electronic structures, we performed first-principles calculations on 2D VO_2(M) nanostructures based on the atomic structures extracted from EXAFS. The structural model of the VO_2(M) single layer is shown in Figure 3c, which have a circa 5 Å thickness, and we thus built a six-monolayer VO_2(M) slab model to meet the thickness of the as-synthesized ultrathin nanosheet. The increased symmetry of V–V chain is shown in the relaxed structure in the plane model. The calculated density of states (DOSs) are shown in Figure 3d. Clearly, the bulk VO_2(M) is a semiconductor, showing the band gap of about 0.65 eV, in agreement with experimental and calculation results in literature.[25] However, for the six-monolayer configuration of VO_2(M), we can find that the spin-down states show a band gap of about 0.41 eV, whereas the spin-up states are gapless. This strongly indicates that the ultrathin nanosheet possesses a half-metallic conductive nature, a desired property in enormous spintronic devices.

Reducing the dimensionality of VO_2(M) from bulk to the ultrathin 2D structure significantly alters its electronic structure from semiconducting/insulating to half-metallic state. From the aspect of the atomic structure, as revealed by XAFS results, the surface distortion of nanosheets supported the minimization of the surface energy and thus would inevitably influence their electronic properties. The higher surface symmetry implies that the surface is more close to the metallic state compared with the interior, as the V–V distance (2.99 Å) is close to the critical distance (2.94 Å) that is required to lead to the itinerant electronic behavior.[25] The spin band structure along high symmetry gives the metallic channel, while that along low symmetry produces the insulating/semiconducting channel. On the other hand, the effects of quantum confinement may also give rise to a new electronic state. For instance, the first-principles calculations by Pardo et al. have also found that quantum confinement of the VO_2(M) slab down to about 1 nm can produce an unexpected half-metallic character.[12] Nagashima et al. has found that a minimum thickness of 5 nm of VO_2(M) film is needed to sustain the insulating state.[26] These mean that the

conductive properties of VO_2(M) depend strongly on its thickness. This can be considered that a collective structural dimerization along the rutile *c* axis is required for the insulating state, which however is inhibited by confinement in thinner layers. As a result, the unique surface distortion and the quantum confinement endow ultrathin VO_2(M) nanosheets with an excellent electronic structure of half-metallicity.

Apart from presenting half-metallicity, ultrathin VO_2(M) nanosheets also have the desired thermally induced SPT, as their bulk counterpart does. However, the traditional variable-temperature XRD, differential scanning calorimetry (DSC), and resistance measurements for identification of the insulator-to-metal transition (IMT) accompanied with SPT are only performed on the bulk sample.[27] Fortunately, the far-IR spectroscopy with the advantage of excluding the influence of the grain boundaries provides sensitive spectral response to the intrinsic lattice vibrations during the phase transition of finite-sized nanomaterials.[28,29] As shown in Figure 4, we found that, for both of the nanosheet and the bulk, the IR transmittance shows strong steplike peaks (ca. 400–1000 cm^{-1}) with sharp maximum at around 873 cm^{-1}. These absorption peaks are the characteristics for V–O vibrations that arise from the asymmetrical VO_6 octahedral in monoclinic phase below T_C.[30,31] Increasing the temperature across T_C, these characteristic absorptions at lower wavenumbers are significantly weakened, and the transmittance at all wavenumbers are decreased, which is due to the formation of rutile structure with higher symmetry. The evolutions of IR transmittances indicate that the VO_2(M) nanosheets also display the thermally induced monoclinic-to-rutile structure transition. The XAFS spectra can also provide the direct evidence for the SPT. As shown in Figure 3b, the XAFS FT curve for the nanosheets measured at 80 °C displays the identical spectral features with those for the tetragonal rutile phase,[24] confirming the structural transition from monoclinic to rutile phases. Notably, the nanosheets show higher transmittance compared with its bulk analogue (Figure 4a, inset). The higher symmetry for the V–V pairs and the [VO_6] octahedron could damp the lattice vibrations, and thus reduce the infrared absorption of V–V and V–O vibrations. Further, the thinner thickness in nanosheet can also decrease the light absorption. These synergistic effects between the microscopic atomic structure and macroscopic morphological features contribute to the higher transmittance in the far-IR region.

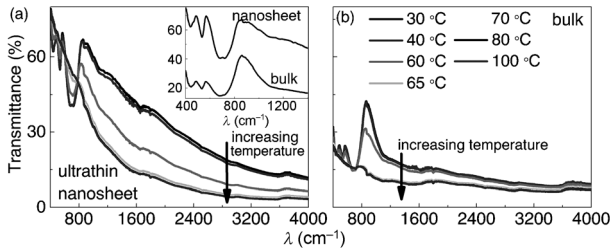

Figure 4. Variable-temperature far-IR spectra of a) ultrathin VO_2(M) nanosheets and b) bulk VO_2(M). The insert compares the far-IR spectrum of a nanosheet and the bulk at room temperature.

In summary, we have demonstrated a facile method to fabricate large-area ultrathin VO_2(M) nanosheets with an average thickness of about 3 nm by lithiation in the M phase followed by the exfoliation in the R phase. We show that the Li intercalation and exfoliation–deintercalation can be finely controlled by exploring the structural activation across characteristic M/R phase transition. The as-obtained nanosheet shows a unique electronic state of half-metallic character that is induced by surface structure distortion and quantum confinement. The thermally induced monoclinic-to-rutile SPT in VO_2(M) nanosheets is successfully demonstrated by variable-temperature far-IR spectra. Such free-standing ultrathin VO_2(M) nanosheets with half-metallicity are expected to be useful for applications in spintronic nanoelectric devices.

Received: April 8, 2013
Revised: May 13, 2013
Published online: June 11, 2013

Keywords: half metallicity · nanosheets · phase transitions · vanadium dioxide

[1] M. Nakano, K. Shibuya, D. Okuyama, T. Hatano, S. Ono, M. Kawasaki, Y. Iwasa, Y. Tokura, *Nature* **2012**, *487*, 459–462.
[2] M. K. Liu, H. Y. Hwang, H. Tao, A. C. Strikwerda, K. B. Fan, G. R. Keiser, A. J. Sternbach, K. G. West, S. Kittiwatanakul, J. W. Lu, S. A. Wolf, F. G. Omenetto, X. Zhang, K. A. Nelson, R. D. Averitt, *Nature* **2012**, *487*, 345–348.
[3] M. Imada, A. Fujimori, Y. Tokura, *Rev. Mod. Phys.* **1998**, *70*, 1039–1263.
[4] T. Driscoll, H. T. Kim, B. G. Chae, B. J. Kim, Y. W. Lee, N. M. Jokerst, S. Palit, D. R. Smith, M. Di Ventra, D. N. Basov, *Science* **2009**, *325*, 1518–1521.
[5] T. S. Kasırga, D. Sun, J. H. Park, J. M. Coy, Z. Y. Fei, X. D. Xu, D. H. Cobden, *Nat. Nanotechnol.* **2012**, *7*, 723–727.
[6] T. Dietl, *Nat. Mater.* **2010**, *9*, 965–974.
[7] S. A. Wolf, D. D. Awschalom, R. A. Buhrman, J. M. Daughton, S. von Molnar, M. L. Roukes, A. Y. Chtchelkanova, D. M. Treger, *Science* **2001**, *294*, 1488–1495.
[8] H. Y. Hwang, S. W. Cheong, *Science* **1997**, *278*, 1607–1609.
[9] J. Feng, X. Sun, C. Z. Wu, L. L. Peng, C. W. Lin, S. L. Hu, J. L. Yang, Y. Xie, *J. Am. Chem. Soc.* **2011**, *133*, 17832–17838.
[10] Z. W. Wang, C. Schliehe, T. Wang, Y. Nagaoka, Y. C. Cao, W. A. Bassett, H. M. Wu, H. Y. Fan, H. Weller, *J. Am. Chem. Soc.* **2011**, *133*, 14484–14487.
[11] Y. W. Son, M. L. Cohen, S. G. Louie, *Nature* **2006**, *444*, 347–349.
[12] V. Pardo, W. E. Pickett, *Phys. Rev. Lett.* **2009**, *102*, 166803.
[13] X. D. Zhang, J. J. Zhang, J. Y. Zhao, B. C. Pan, M. G. Kong, J. Chen, Y. Xie, *J. Am. Chem. Soc.* **2012**, *134*, 11908–11911.
[14] E. J. Kan, W. Hu, C. Y. Xiao, R. F. Lu, K. M. Deng, J. L. Yang, H. B. Su, *J. Am. Chem. Soc.* **2012**, *134*, 5718–5721.
[15] A. Tselev, E. Strelcov, I. A. Luk'yanchuk, J. D. Budai, J. Z. Tischler, I. N. Ivanov, K. Jones, R. Proksch, S. V. Kalinin, A. Kolmakov, *Nano Lett.* **2010**, *10*, 2003–2011.
[16] C. Z. Wu, J. Dai, X. D. Zhang, J. L. Yang, F. Qi, C. Gao, Y. Xie, *Angew. Chem.* **2010**, *122*, 138–141; *Angew. Chem. Int. Ed.* **2010**, *49*, 134–137.
[17] J. Nag, R. F. Haglund, *J. Phys. Condens. Matter* **2008**, *20*, 264016.
[18] L. Liu, T. Yao, X. G. Tan, Q. H. Liu, Z. Q. Wang, D. C. Shen, Z. H. Sun, S. Q. Wei, Y. Xie, *Small* **2012**, *8*, 3752–3756.

[19] A. C. Jones, S. Berweger, J. Wei, D. Cobden, M. B. Raschke, *Nano Lett.* **2010**, *10*, 1574 – 1581.
[20] A. Tselev, J. D. Budai, E. Strelcov, J. Z. Tischler, A. Kolmakov, S. V. Kalinin, *Nano Lett.* **2011**, *11*, 3065 – 3073.
[21] Z. S. Tao, T. R. T. Han, S. D. Mahanti, P. M. Duxbury, F. Yuan, C. Y. Ruan, K. Wang, J. Q. Wu, *Phys. Rev. Lett.* **2012**, *109*, 166406.
[22] L. Whittaker, C. Jaye, Z. G. Fu, D. A. Fischer, S. Banerjee, *J. Am. Chem. Soc.* **2009**, *131*, 8884 – 8894.
[23] J. Cao, E. Ertekin, V. Srinivasan, W. Fan, S. Huang, H. Zheng, J. W. L. Yim, D. R. Khanal, D. F. Ogletree, J. C. Grossmanan, J. Wu, *Nat. Nanotechnol.* **2009**, *4*, 732 – 737.
[24] T. Yao, X. D. Zhang, Z. H. Sun, S. J. Liu, Y. Y. Huang, Y. Xie, C. Z. Wu, X. Yuan, W. Q. Zhang, Z. Y. Wu, G. Q. Pan, F. C. Hu, L. H. Wu, Q. H. Liu, S. Q. Wei, *Phys. Rev. Lett.* **2010**, *105*, 226405.
[25] S. Biermann, A. Poteryaev, A. I. Lichtenstein, A. Georges, *Phys. Rev. Lett.* **2005**, *94*, 026404.
[26] K. Nagashima, T. Yanagida, H. Tanaka, T. Kawai, *J. Appl. Phys.* **2007**, *101*, 026103.
[27] Y. Gao, H. Luo, Z. Zhang, L. Kang, Z. Chen, J. Du, M. Kanehira, C. Cao, *Nano Energy* **2012**, *1*, 221 – 246.
[28] L. Zheng, W. Su, Z. Qi, Y. Xu, M. Zhou, Y. Xie, *Nanotechnology* **2011**, *22*, 485706.
[29] Y. F. Sun, B. Y. Qu, S. S. Jiang, C. Z. Wu, B. C. Pan, Y. Xie, *Nanoscale* **2011**, *3*, 2609 – 2614.
[30] Y. F. Sun, S. S. Jiang, W. T. Bi, R. Long, X. G. Tan, C. Z. Wu, S. Q. Wei, Y. Xie, *Nanoscale* **2011**, *3*, 4394 – 4401.
[31] K. W. Lee, J. J. Kweon, C. E. Lee, A. Gedanken, R. Ganesan, *Appl. Phys. Lett.* **2010**, *96*, 243111.

